Thermo-mechanical behavior of EUV pellicle under dynamic exposure conditions

Dario L. Goldfarb[1*], Max O. Bloomfield[2] and Matthew Colburn[3]

[1] IBM T.J.Watson Research Center, 1101 Kitchawan Rd., Yorktown Heights, NY 10598

[2] Scientific Computation Research Center, Rensselaer Polytechnic Institute, 110 8th St., Troy, NY 12180

[3] IBM Research - Albany Nanotech, 257 Fuller Rd., Albany, NY 12203

ABSTRACT

The utilization of EUV pellicles as protective layers for EUV masks requires the use of refractory materials that can tolerate large temperature excursions due to the non-negligible absorption of EUV radiation during exposure. Additionally, the mechanical stress induced on the EUV pellicle by the thermal load is dependent on the thermal expansion of the material which can be responsible for transient wrinkling. In this study, an ultrathin (20 nm), free-standing membrane based on silicon nitride is utilized as a learning vehicle to understand the material requirements of EUV pellicles under dynamic exposure conditions that are typical of commercial EUV scanners. First, the nanoscale radiative properties (emissivity) and thermo-mechanical failure temperature of the dielectric film under vacuum conditions are experimentally investigated utilizing a pulsed ArF (193 nm) probing laser. The silicon nitride membrane is found to be marginally compatible with an equivalent 80W EUV source power under steady state illumination conditions. Next, the thermal behavior of the EUV pellicle under dynamic exposure conditions is simulated using a finite element solver. The transient temperature profile and stress distribution across the membrane under stationary state conditions are extracted for an equivalent 60W EUV power source and the pellicle wrinkling due to heating and consequent impact on CD uniformity is estimated. The present work provides a generalized methodology to anticipate the thermal response of a EUV pellicle under realistic exposure conditions.

Keywords: EUV mask infrastructure ; EUV pellicle ; Silicon nitride ; Dynamic exposure conditions ; Nanoscale emissivity ; Membrane wrinkling

1. INTRODUCTION

1.1 Thermal Study of EUV pellicle - Motivation

EUV pellicles consisting of thin unsupported membranes are intensively sought after by early users of EUV scanners as a protective barrier against particle contamination of EUV photomasks during use, storage and transport. The study of EUV pellicle materials under realistic EUV exposure conditions requires the careful consideration of their mechanical, thermal and chemical response to inertial displacement and EUV radiation absorption under vacuum conditions as found inside the EUV scanner. Particularly, the transient heating of the free-standing membrane arising from EUV radiation absorption results in film expansion and temporary tensility loss due to the positive coefficient of thermal expansion (CTE), which can result in detrimental pellicle wrinkling and ultimately impact critical dimension uniformity (CDU) during EUV imaging. Furthermore, the cyclic pellicle heating-cooling can make the EUV pellicle material prone to fatigue as alternated compressive-tensile stress is repeatedly induced in the suspended membrane during EUV exposures.

[*] goldfarb@us.ibm.com; phone (914) 945 1308

Extreme Ultraviolet (EUV) Lithography VII, edited by Eric M. Panning, Proc. of SPIE Vol. 9776, 977621 · © 2015 SPIE · CCC code: 0277-786X/15/$18 · doi: 10.1117/12.2218453

Downloaded From: http://proceedings.spiedigitallibrary.org/ on 03/24/2016 Terms of Use: http://spiedigitallibrary.org/ss/TermsOfUse.aspx

The sharp temperature rise upon EUV radiation absorption by a EUV pellicle based on polycrystalline silicon (pSi) has been described at length [1-4], and the concomitant pellicle wrinkling and image fidelity limit have been analytically determined [5]. Similarly, the thermal durability of pSi as a pellicle material has been recently investigated, and the observed structural changes upon thermal cycling have been attributed to grain boundary split, creep deformation, thermal softening and micro-cracking among other possible factors [6-8].

In this work, an ultrathin (20 nm), free-standing membrane based on silicon nitride (SiN_x) is used as a model EUV pellicle to understand the thermo-mechanical response of refractory materials to dynamic EUV exposure conditions. SiN_x has been adopted as a capping layer for the pSi-based EUV pellicle, and the fabrication of a full size (113x145 mm) SiN_x EUV pellicle has been recently demonstrated [9]. A large body of information is available regarding the compositional, physical, thermal, mechanical and optical properties of SiN_x, thus making it suitable as a learning vehicle to understand the practical limitations of unsupported films featuring ultralarge area-to-thickness ratios as EUV pellicles.

2. BACKGROUND

2.1 EUV Pellicle – Radiative Properties at the Nanoscale

The thermal balance for a single pellicle material exposed to EUV radiation in a EUV scanner is comprehensively described by the following differential equation based upon Figure 1:

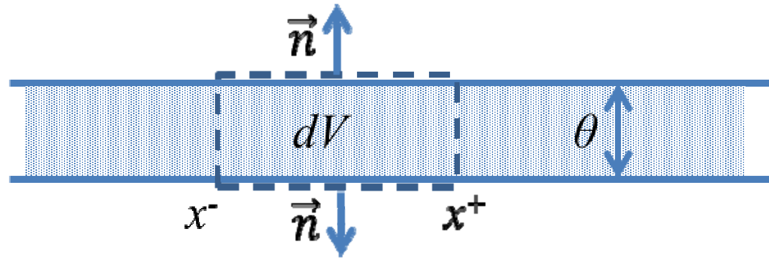

Figure 1. Schematic of control volume dV on pellicle used to obtain a thermal balance. θ is the film thickness and $\vec{n}$ are outward facing normals from the surface of the pellicle.

$$\rho C_{\rm p} dV \frac{dT}{dt} = H_{\rm EUV}(\vec{r},t)dV - \varepsilon\sigma_{\rm SB}T^4\vec{n}\cdot dV + \varepsilon\sigma_{\rm SB}T_\infty^4(\vec{n}\cdot dV) + k_T T\theta[\nabla T(x^+) - \nabla T(x^-)] - H_{\rm diff}\frac{dV}{\theta} \qquad (1)$$

where the left side represents the total thermal energy accumulation rate in a small control volume dV, as shown in Figure 1. On the left hand side, ρ is the mass density, C_p is the specific heat of the pellicle material, T is the local pellicle temperature, and t is the time. On the right side, H_{EUV} is the volumetric EUV energy absorption rate, ε is the emissivity, σ_{SB} is the Stefan-Boltzmann constant (5.67×10^{-12} W cm^{-2} K^{-4}), $\vec{n}$ is the outward facing normal from the pellicle surface, T_∞ is the temperature of the surroundings, k_T is the thermal conductivity of the pellicle, θ is the film thickness, x^- and x^+ represent the negative and positive positions of the control volume, and H_{diff} represents the areal heat transfer rate to any surrounding gas.

The five terms on the right of this balance represent, respectively, EUV absorption, Stefan-Boltzmann thermal radiation from the film, Stefan-Boltzmann thermal radiation to the film from the environment in the scanner, Fourier heat conduction in the plane of the film, and diffusive heat transfer from the film by any surrounding gas. In-plane heat conduction is negligible across the ultrathin pellicle and heat diffusion via gas cooling can be disregarded due to the high vacuum environment. At elevated temperatures, associated with EUV absorption, $T >> T_\infty$ and the radiative heat transfer to the film from the chamber is dwarfed by the radiative heat transfer from the film. Therefore, in our initial experiments the last three terms on the right side of the equation (1) can be neglected, leaving the radiative mechanism as the dominant path through which heat can be removed from the EUV pellicle.

Downloaded From: http://proceedings.spiedigitallibrary.org/ on 03/24/2016 Terms of Use: http://spiedigitallibrary.org/ss/TermsOfUse.aspx

The ultrathin nature of the pellicle film becomes important through the emissivity, which relates the thermal emission of the radiating object to that of a perfectly black body -a surface property that depends on the specific material, the surface roughness, and the radiating temperature. Deviations from the classical blackbody radiation described by Stefan-Boltzmann's law start to occur when radiating objects become smaller than the peak thermal wavelength, $\lambda_T = \hbar c / k_B T$, (~7.6 μm at room temperature) [10]. In the case of radiating materials with dimensions smaller than λ_T a correction to the Stefan-Boltzmann law can be accommodated with a suitable choice of ε that accounts for the *microscopic* dimensions of the radiating object [11]. For the case of EUV pellicles, radiative heat dissipation becomes substantially overestimated if bulk emissivity values are used, resulting in an underestimate of the attained pellicle temperature upon EUV radiation absorption.

An additional parameter that needs to be taken into account is the absorption length or penetration depth (δ) of the emitted radiation. For an object with at least one *nanoscopic* dimension (*e.g.* radius, thickness) smaller than δ, it is useful to formulate a complex refractive index ($\tilde{n} = n - ik$), where the imaginary part (k) is the single material property that dictates the spectral emissivity. Due to the nature of the radiated energy spectrum, the infrared (IR) region is directly associated with the emissive and absorptive properties of the radiating object. Namely, a hypothetical EUV pellicle with purely real dielectric functions in the IR region (*i.e.* $k_{IR} = 0$) would neither absorb nor radiate heat at any pellicle thickness, due to the lack of dissipative properties of the material. Dielectric materials (insulators) are characterized by their poor radiative properties arising from a modest spectral absorptivity in the IR region, and their use as EUV pellicle materials has been limited to the ultrathin film comprising the capping layer. Conversely, electrically conductive materials (*e.g.* metals, graphite) can radiate a larger amount of heat due to a larger imaginary part of the dielectric function compared to insulating materials of equivalent thickness, and are finding use as effective heat dissipation layers for EUV pellicles [7,8,12,13].

For EUV pellicles comprised of a dielectric material (*e.g.* SiO_2, SiN_x, SiC), the radiated heat is expected to be proportional to their thickness as well as their projected area, that is to say, proportional to their volume [10]. The θ dependence vanishes in the macroscopic domain, where the Stefan-Boltzmann law can be applied using bulk emissivity values, indicating that the radiated heat originates from a finite skin depth on the membrane surface. This skin depth is related to the absorption length (δ) of the *dielectric* membrane for the IR spectrum, which in turn is directly connected to the optical properties of the radiating membrane material. Indeed, as soon as the absorption length (δ) for the IR spectrum becomes larger than the thickness (θ) of the radiating *dielectric* membrane, thermal radiation becomes a volumetric effect and the emissivity (ε) has to take the photonic properties of the *dielectric* EUV pellicle material into account [14]. In other words, EUV pellicle emissivity is dependent on the thickness of the free-standing dielectric membrane due to the nanoscale dimension.

Conductors such as metals (*e.g.* gold, tungsten) differ from insulators by a significantly smaller skin depth, leading to very different radiation characteristics. In the limit of nanoscopic thickness, dielectrics emit proportional to their volume, but this regime is not reached for metals in the thickness range applicable to EUV pellicle technology (<10nm). Instead, the radiation per unit area can be very large for metals in the nanoscale regime, exceeding the value expected from the areal-proportionality of the Stefan-Boltzmann law. A maximum occurs where the metal thickness is roughly equal to the skin depth ($\theta \sim \delta$), as each volume element radiates strongly, but re-absorption within the volume is still small [10].

Examples of δ values for dielectric and conducting materials are given in Table 1. It is noteworthy that if a pellicle with EUV transmission equal to or larger than 90% (single pass) is desired, the condition $\theta < \delta$ is observed for all EUV pellicle material options and the volumetric effect needs to be carefully considered.

Table 1. Absorption length (δ) and pellicle thickness corresponding to EUV transmission equal to 90% single pass (θ_{90}) for selected dielectric and conducting materials [10].

Material	SiO2	SiC	Graphite	Gold	Tungsten
δ (nm)	570	128	100	20	10
θ_{90} (nm)	8.7	23.5	15.8	2.2	2.7

Downloaded From: http://proceedings.spiedigitallibrary.org/ on 03/24/2016 Terms of Use: http://spiedigitallibrary.org/ss/TermsOfUse.aspx

3. EXPERIMENTAL

3.1 EUV Pellicle – Heat Load Test Stand

Heat-load tests of EUV pellicle materials are typically conducted by exposing the suspended membrane to sequentially increasing laser power under vacuum conditions in order to simulate actual EUV source power. Typical laser wavelengths utilized are in the UV (*e.g.* 355 nm) or visible (*e.g.* 405 nm, 532 nm, 810 nm) ranges. However, laser heating of a EUV pellicle based on SiN_x is particularly difficult to accomplish at $\lambda > 350$nm due to its low absorptivity.

In this work, an ArF excimer laser ($\lambda = 193$ nm) was used to irradiate and efficiently heat a EUV pellicle based on SiN_x placed inside an evacuated exposure chamber in an inert atmosphere. The ArF laser setup consisted on a pulsed beam with tunable repetition rate (*f*) and pulse energy (nominal pulse duration of 12ns, FWHM). The entire beamline was purged with nitrogen (N_2) gas in order to minimize ArF radiation absorption by atmospheric oxygen. A flip mirror allowed for the laser beam to be directed to a thermopile-based device which was used to monitor the total laser power (Figure 2). The laser was operated at minimum nominal pulse energy in order to provide a more uniform time-averaged heating of the EUV pellicle. Actual laser pulse energy was obtained by dividing the measured total laser power by the repetition rate, and was found to be invariant (0.15 ± 0.01 mJ/pulse) at repetition rates above 100 Hz.

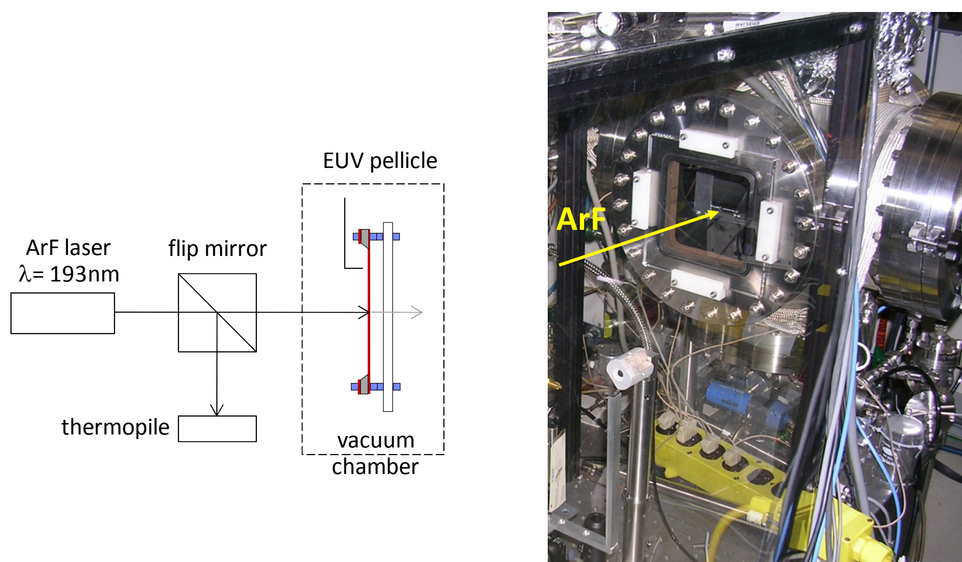

Figure 2. ArF exposure setup used for heat load testing of EUV pellicle based on SiNx. Left: schematic diagram. Right: actual vacuum exposure chamber.

At a laser power of 80 mW and a repetition rate of 500 Hz, power actually delivered by the ArF laser was found to be spatially non-uniform at the imaging plane where the pellicle was positioned. Because limited heat conduction in the plane of the ultrathin SiNx membrane was expected, the spatial energy distribution deposited in the EUV pellicle was consequently measured and the maximum power intensity distribution of the laser spot (peak ArF laser power) was quantitatively determined.

Power mapping of the ArF laser beam was done by resorting to a photoresist film as a dose monitor. A silicon wafer was coated with a commercial ArF bottom antireflective coating (BARC) and a positive-tone ArF resist, mounted in place of the EUV pellicle and exposed to the ArF laser beam through a chrome-on-glass attenuator for various lengths of time (t_i). A post-exposure bake (PEB) followed by aqueous development, rinsing and drying revealed a cleared resist spot with area proportional to the exposure time. Due to the known high contrast of the ArF resist, the edge of the exposure spot can be unequivocally assigned a dose value equal to the dose-to-clear (*DtC*) while the inner region of the cleared resist area remains overexposed (dose > *DtC*). Thickness mapping of the resist film was followed by calculation of the cleared resist areas (A_i) for the different exposure times (Figure 3).

Downloaded From: http://proceedings.spiedigitallibrary.org/ on 03/24/2016 Terms of Use: http://spiedigitallibrary.org/ss/TermsOfUse.aspx

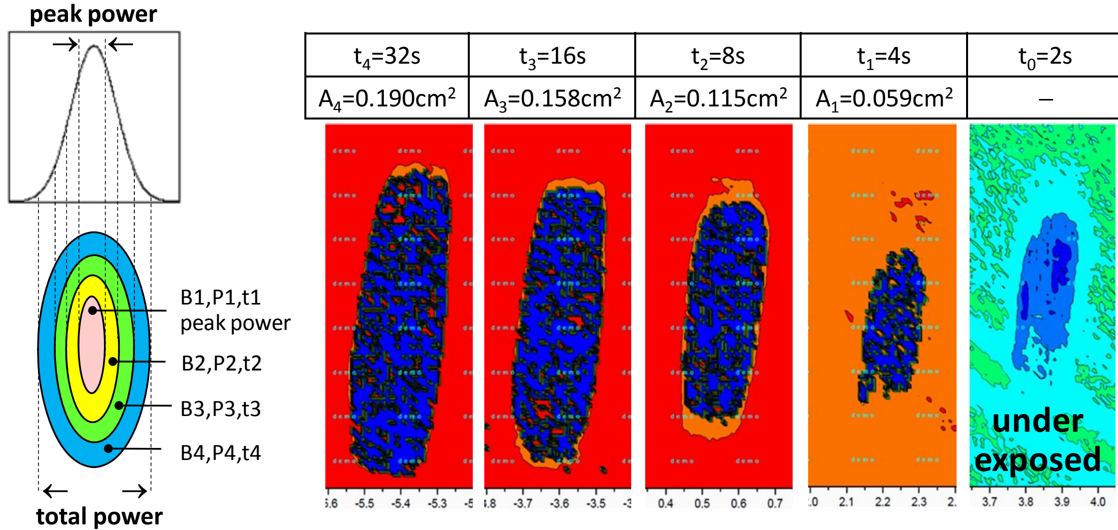

Figure 3. Method applied to the determination of peak ArF laser power per unit area (P_1/A_1) using a photoresist as a dose monitor and a timed exposure. Dark blue regions correspond to zero resist thickness. Rightmost exposure is underexposed (dose < *DtC*).

Upon inspection of the different exposure spots it is possible to approximate the total laser beam area as the cleared resist area A_4 (0.190 cm^2) associated with the longest exposure time, t_4 (32 s), since there is little additional increase in the exposed area upon a significant increase in the exposure time from t_3 (16 s) to t_4. The laser spot may then be partitioned into individual bands with band areas (B_i) and band powers (P_i) that can be equated to:

$$B_i = A_i - A_{i-1} \tag{2}$$

$$P_i = P_{i-1}\frac{t_{i-1}}{t_i} \tag{3}$$

Note that the calculation of an individual band power is independent of the dose delivered to the photoresist through the attenuator, since the mapped resist spots serve the sole purpose of obtaining the individual band areas. The contribution of these bands to the total power is then calculated as:

$$P_{\text{total}}A_{\text{total}} = \sum P_i B_i = P_1\left(B_1 + B_2\frac{t_1}{t_2} + B_3\frac{t_1}{t_3} + B_4\frac{t_1}{t_4}\right) \tag{4}$$

Inserting the measured values into equation (4), a peak ArF laser power per unit area (P_1/A_1) equal to 2.56 W/cm^2 is calculated when delivering a total laser power of 80 mW.

3.2 EUV Pellicle – Measuring Nanoscale Emissivity

The ultimate peak power that a SiNx membrane can tolerate was experimentally determined utilizing the ArF laser exposure system described above. A EUV pellicle (SiNx, 20nm) was placed inside the exposure chamber and the N_2 pressure was reduced to $< 10^{-4}$ mbar. The laser frequency was gradually increased while operating at minimum nominal laser pulse energy (0.15 mJ/pulse) at the same time as the physical integrity of the pellicle was visually monitored. Evidence of pellicle heating was first detected at f = 160 Hz, revealed by visible glowing of the SiNx membrane. Pellicle failure occurred at f = 200 Hz, equivalent to a total laser power of 30 mW and a peak laser power per unit area equal to 0.96 W/cm^2 delivered to the pellicle. The fraction of ArF radiation absorbed by the pellicle was equal to 42%, calculated using IMD software [15] and the experimentally measured optical constants (*n,k*) of the SiNx layer at

Downloaded From: http://proceedings.spiedigitallibrary.org/ on 03/24/2016 Terms of Use: http://spiedigitallibrary.org/ss/TermsOfUse.aspx

λ= 193nm [9] under normal incidence. The ArF laser power absorption per unit area leading to thermal failure of the EUV pellicle is thus calculated to be 42% of 0.96 W/cm^2 or 0.40 W/cm^2.

Accurate detection of the EUV pellicle temperature using a pyrometer or thermal imaging camera is not possible due to the large departure of the nanoscale spectral emissivity from the bulk value for the heated specimen. Instead, pellicle thermal failure was ascribed to silicon nitride decomposition upon melting occurring at T_m= 1850°C (2123 K) [16].

Applying the Stefan-Boltzmann law with this power absorption and this temperature, we can calculate an effective nanoscale emissivity of 0.0035. It is noted that the obtained value is only applicable to a SiN_x membrane with thickness equal to 20 nm, due to the volumetric effects mentioned in Section 2. The nanoscale SiNx emissivity reported in this work is starkly lower than the bulk emissivity of silicon nitride (ε = 0.87-0.98) informed at 135°C and 805°C [17], which is found to be temperature-invariant. The value herein reported constitutes the first experimental determination of the nanoscale emissivity of a EUV pellicle at elevated temperature (1850°C). The high-temperature emissivity of the 20nm SiNx membrane determined in this work is in good agreement with the emissivity of a silicon nitride film with thickness equal to 50nm (ε = 0.008) measured at 100°C and reported elsewhere [8], which supports the thickness dependence previously described.

3.3 EUV Pellicle – EUV Source Power Compatibility

The heat load test results obtained in Section 3.2 can be directly applied to predict the compatibility of the SiNx pellicle with EUV sources of different power. Ultimate compatibility is given by the ability of the pellicle to remain at a steady state temperature below the material operating limit upon EUV radiation absorption.

The limiting amount of generated heat (H_{fail} = 0.40 W/cm^2) formerly obtained can be compared with the total EUV power absorbed by the 20nm SiNx pellicle (Table 2), taking into account the expected incident power on the pellicle for different EUV source power values. Pellicle failure under vacuum exposure conditions is expected at a total EUV incident power equal to 1.85 W/cm^2 (equivalent to an 82W EUV source power). Therefore, a 20nm SiNx EUV is only marginally compatible with the presently deployed commercial EUV sources with nominal EUV power equal to 80W, indicating that pellicle materials with improved heat dissipation properties compared to SiNx are required.

Table 2. EUV source–pellicle compatibility calculated for a 20nm SiNx membrane.

EUV Source	S0	S1		S2	S3
EUV Source Power (W)	**40**	**60**	**80**	**125**	**250**
SiNx Thickness (nm)	20	20	20	20	20
Pellicle Absorption, single pass (%)	14	14	14	14	14
Emissivity (SiNx, 20nm)	0.0035	0.0035	0.0035	0.0035	0.0035
Incident EUV Power on pellicle (W/cm^2) [6]	0.90	1.34	1.79	2.80	5.60
Absorbed EUV power, first pass (W/cm^2)	0.13	0.19	0.25	0.39	0.78
Reflected EUV Power on Mask (W/cm^2)	0.50	0.75	1.00	1.57	3.13
Absorbed EUV power, second pass (W/cm^2)	0.07	0.10	0.14	0.22	0.44
Total absorbed EUV power (W/cm^2)	**0.20**	**0.29**	**0.39**	**0.61**	**1.22**
Steady State Temperature (°C)	**1499**	**1688**	**1834**	**2083**	**2528**
SiNx Operating Limit (°C) [16]	**1850**				

4. MODELING

4.1 Pellicle Heating Under Dynamic Exposure Conditions

During actual device patterning using projection-reduction lithography, radiation is allowed to propagate through a narrow slit while the wafer and the photomask are synchronously scanned. In the case of EUV exposures the slit is curved to minimize aberrations. The scanning motion creates a novel heat transfer problem, and although no steady

Downloaded From: http://proceedings.spiedigitallibrary.org/ on 03/24/2016 Terms of Use: http://spiedigitallibrary.org/ss/TermsOfUse.aspx

state can be reached because the EUV exposure is periodic in time, a stationary state can be determined. This stationary state is not a single temperature profile, but a periodic time series of temperature profiles, after start-up transients have damped out. To determine this stationary state, the non-equilibrium heat transfer equation is formulated point-wise over the area of the pellicle, along with its accompanying boundary condition.

$$\rho C_p \frac{dT}{dt} = k_T \nabla^2 T - \varepsilon \sigma_{\mathrm{SB}} T^4 + \varepsilon \sigma_{\mathrm{SB}} T_\infty^4 + H_{\mathrm{EUV}}(\vec{r}, t) \quad (5)$$

$$\vec{\mathrm{n}} \cdot \nabla T(\Gamma) = 0 \quad (6)$$

In the boundary condition (Equation 6), Γ represents the boundary where the pellicle meets the frame, and $\vec{n}$ now represents the normal vector at that boundary. This equation is equivalent to an adiabatic boundary condition at the pellicle boundary. In this dynamic model, conductive heat transfer within the plane of the pellicle is accounted for, though the temperature profile is taken to be uniform through the thickness of the pellicle due to its small length scale. Similarly, radiative heat transfer from the surroundings to the pellicle is reintroduced, which stabilizes the baseline temperature of the simulated pellicle over long times, despite the purely adiabatic boundary conditions.

To solve this equation, the standard finite element "weak form" of the equation is developed by multiplying by a weighting function and integrating over elements which partition the domain [18]. This weak form is then discretized in time, using a forward differencing scheme, and the resulting time and space discretized form is then implemented in DOLFIN [19], an automated finite element development package that is part of the open source FEniCS Project [20]. In DOLFIN, the pellicle is discretized with a 2D mesh containing ~3000 linear quadrilateral elements and integrated using a time step of 10^{-3} s. The material and exposure parameters used are given in Table 3 and Table 4 respectively. The product (throughput)×(chips/wafer)×(reticle passes/chip)×(scanned distance/reticle pass)×(overhead) was calculated to obtained the reticle speed.

Table 3. Micro-nanoscale thermophysical properties of silicon nitride.

Parameter	Value	Measurement Temperature	Specimen Dimension	Material	Reference
Heat Capacity	0.7 J/(g.K)	300K	2-4 μm *	(A)	[21]
Density	3.0 g/cm^3	300K	2-4 μm *	(A)	[21]
Young's Modulus	300-365 GPa	300K	300nm **	(A)	[22]
Thermal Expansion	3.2x10^{-6} ppm/K	573K	300nm ***	(A)	[22]
Thermal conductivity	0.025 W/(cm.K)	300K	50nm *	(B)	[23]
Emissivity	0.0035	~ 2000K	20nm **	(A)	this work

(A): Amorphous low-stress Si-rich LPCVD SiNx; (B): LPCVD Si_3N_4, variable strain.
*Bridge geometry; **Membrane geometry; ***Film geometry

Table 4. EUV scanning exposure parameters used for computational modeling.

Reticle speed	0.4 m/s	EUV source power	60 W
Throughput	60 wph	EUV power absorbed	0.29 W/cm^2
Chips/wafer	150	Illumination ring (slit)	110.7 mm x 8 mm
Reticle passes/chip	1	Dwell time (chip-to-chip)	0.05 s
Distance/reticle pass	144 mm	Maximum reticle acceleration	100 m/s^2
Overhead fraction	10%	Pressure inside scanner	vacuum

Figure 4 shows a computed temperature profile of the pellicle at 0.25s after start-up. It is observed that start-up transients are short lived on the time scale of a single sweep of the slit. One-dimensional simulations in the direction of slit travel produced very similar results to 2D simulations, showing that the effect of curvature of the slit on temperature profile is small. The strip of high temperature seen in Figure 4 lags the motion of the slit by less than a millimeter,

Downloaded From: http://proceedings.spiedigitallibrary.org/ on 03/24/2016 Terms of Use: http://spiedigitallibrary.org/ss/TermsOfUse.aspx

resulting in a very sharp rise in temperature at the leading edge of the exposure region. The maximum temperature inside the transiently exposed area of the pellicle reaches ~1950K (~1680°C), about 170K below the reported decomposition temperature of silicon nitride (2123K), and is observed to remain constant across a transversal distance of about 6mm, indicating that an instantaneous steady state is locally achieved within the areal slit. Additionally, the temperature drops swiftly towards the background T_∞ temperature of 300K after the slit passes over a location, with temperatures reaching 400K within 0.15s. This very fast cooling may be attributed to the small heat capacity of the thin pellicle.

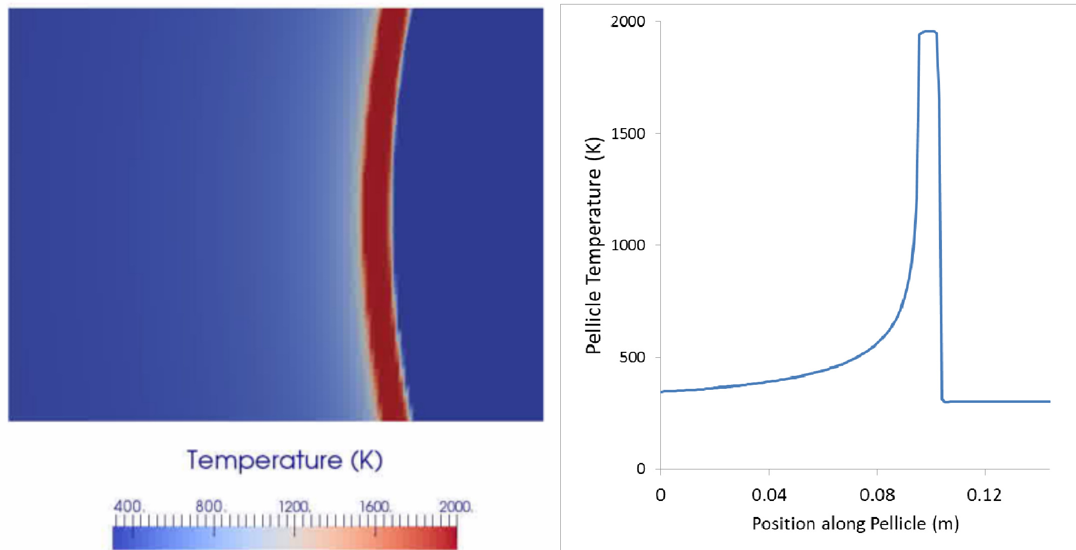

Figure 4. Left: computed temperature profile of the pellicle at 0.25s using the EUV scanning exposure parameters shown in Table 4. Right: temperature along centerline, showing temperature profile in direction of slit travel (left to right) extracted from 2D result, also at 0.25s.

4.2 EUV Pellicle Wrinkling Impact on Imaging

The consequent thermal expansion of the EUV pellicle upon heating by EUV radiation absorption is expected to result in membrane wrinkling if the intrinsic tensile stress is overcome and the membrane is transiently placed under compression in the direction orthogonal to the slit motion (Figure 5, left). The impact of pellicle wrinkling on EUV image quality has been described in terms of local apodization variability (i.e., EUV transmission angular non-uniformity) and the associated loss of critical dimension uniformity (CDU) [3]. The associated figure of merit is the maximum local angle of a wrinkle ($\theta_{max}=2\pi\ A/\lambda$) which should not exceed 300mrad, in order to maintain a CDU below 0.1nm [5,6].

A complete wrinkling analysis through finite-element modeling (FEM) utilizing shell elements and including buckling modes, taking into account the macroscopic (x,y) and nanoscopic (z) dimensions of the EUV pellicle as well as the time scale attained under dynamic exposure conditions is beyond the scope of this work. Instead, an approximation is made in order to provide a time-independent 2D solution (Figure 5, right). The curved slit is herein replaced by a rectangular area of length (L) equal to the width of the pellicle. The material elongation (ΔL) due to thermal expansion leads to membrane wrinkling, and the resulting wrinkled pellicle surface is approximated either by a sinusoidal or a seesaw wave of variable amplitude (A) and period (λ). The advantage of the proposed model is the resulting analytical solution for the quotient (A/λ), which is only dependent on the pellicle material properties and the delivered EUV power, thus yielding a direct correlation to the impact on imaging performance. The simplified model does not take into account edge effects such as stress concentration near the frame boundary or any possible pellicle buckling [4]. Similarly, strain gradients on the leading edge of the exposure window due to a sharp transition in the temperature profile -which are likely to result in wrinkles [4,24]- are also neglected in the model, thus providing a conservative estimate of wrinkling impact on imaging.

Downloaded From: http://proceedings.spiedigitallibrary.org/ on 03/24/2016 Terms of Use: http://spiedigitallibrary.org/ss/TermsOfUse.aspx

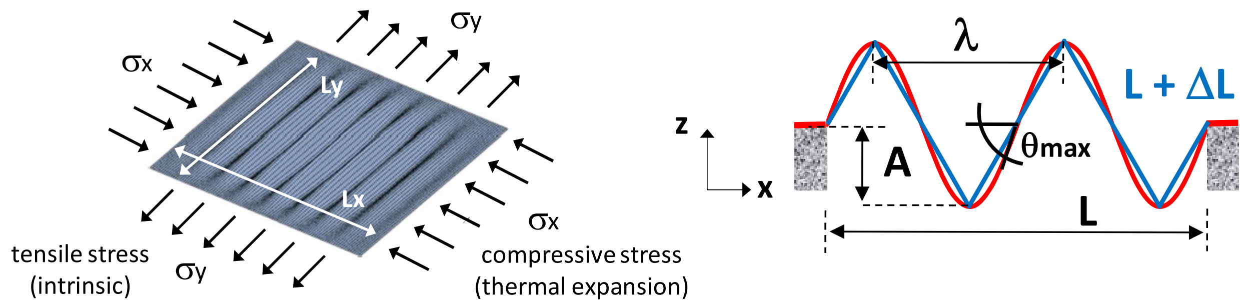

Figure 5. Left: schematic 3D representation of EUV pellicle wrinkling arising from compressive stress (σ_x) perpendicular to the scan direction due to thermal expansion, and intrinsic tensile stress (σ_y) parallel to the scan direction (image adapted from [25]). Right: simplified 2D wrinkling model applying a sinusoidal (red) or seesaw (blue) function.

The calculation of pellicle wrinkling impact on CD uniformity using the described model is implemented by first calculating the temperature ($T_{\sigma=0}$) at which the tensile stress is canceled out by the tensility loss ($\Delta\sigma$) due to pellicle heating and thermal expansion:

$$\Delta\sigma = E\beta(T_{\sigma=0} - T_{\infty}) \tag{7}$$

where E and β are the Young's Modulus and CTE respectively.

Subsequently, the strain ($\Delta L/L$) is calculated based on the material elongation allowed by the CTE up to the steady state temperature (T_{max}):

$$\frac{\Delta L}{L} = \beta(T_{\max} - T_{\sigma=0}) \tag{8}$$

The relationship between $\Delta L/L$ and the quotient (A/λ) is obtained by solving the length of the modeled wrinkle. In the case of a sinusoidal function, the length of the sinusoid is represented by an elliptic integral of the second kind, which can be solved numerically. An approximation using a seesaw function provides a simple analytical solution that is independent of the number of wrinkle periods and yields comparable results within 2% error. Finally, the maximum local angle of a wrinkle ($\theta_{max}= 2\pi A/\lambda$) is straightforwardly obtained, and can be compared to the specification value. For a 20nm SiNx EUV pellicle exposed using a 60W EUV power source, a small pellicle deformation is calculated ($\Delta L/L$=0.44%), producing a tolerable wrinkle angle (θ_{max}= 148mrad) which is within the specification (θ_{max}< 300mrad). It is therefore concluded that despite the elevated temperature reached by the EUV pellicle and the transient compressive stress present during scanning, the estimated pellicle wrinkling is not expected to significantly affect the CDU budget (contribution to CD non-uniformity < 0.1nm).

5. SUMMARY AND OUTLOOK

An ultrathin (20nm) free-standing silicon nitride (SiNx) membrane was fabricated and used as a model to understand the thermomechanical response of an EUV pellicle to dynamic EUV exposure conditions. This model EUV pellicle was studied to determine its nanoscale radiative properties and was found to exhibit a nanoscale emissivity significantly smaller than that of bulk SiNx. To our knowledge, this measurement represents the first experimental determination of the nanoscale emissivity of a EUV pellicle obtained at its operating temperature.

Downloaded From: http://proceedings.spiedigitallibrary.org/ on 03/24/2016 Terms of Use: http://spiedigitallibrary.org/ss/TermsOfUse.aspx

The thermo-mechanical failure temperature of the dielectric film was experimentally investigated under vacuum conditions utilizing a pulsed ArF (193nm) probing laser. The 20nm SiNx membrane was found to be marginally compatible with an equivalent 80W EUV source power under steady state illumination conditions.

A 2D finite element model of the non-equilibrium heat transfer in the pellicle was created to simulate a moving exposure window and heat transfer from a 60W EUV source to the 20nm SiNx EUV pellicle. The modeled EUV pellicle reached a maximum temperature equal to 1950K and a steady state was locally verified within the areal slit.

The consequent impact on EUV imaging from pellicle heating was calculated using a simplified wrinkling model producing an analytical solution for the figure of merit (A/λ) that is only dependent on the pellicle material properties and the delivered EUV power. The presence of the 20nm SiNx EUV pellicle was found to have negligible impact on imaging performance when using a 60W EUV source, according to the wrinkling model described in this work.

Future work includes the incorporation of alternative EUV pellicle materials with improved heat dissipation properties and concomitant EUV and DUV transmission. Learning and capabilities acquired and implemented throughout the course of this work are currently being used as guidelines for such ongoing development.

6. ACKNOWLEDGEMENTS

The authors are indebted to Alfred Wagner and Richard Haight for technical support. This work was partially performed at the Microelectronics Research Laboratory (MRL) at the IBM T.J. Watson Research Center. The authors are grateful to the MRL staff for their contributions to this work. Finally, management support provided by Derren Dunn, Daniel Corliss, and Nelson Felix is gratefully acknowledged.

7. REFERENCES

[1] I-S. Kim, H-C. Lee, E-J. Kim, J-W. Kim and H-K. Oh, “Is extreme ultraviolet pellicle possible? - in terms of heat absorption”, *Proc. SPIE*, Vol. 8322, 83222X (2012).

[2] H-C. Lee, E-J. Kim, J-W. Kim , H-K. Oh, “Temperature behavior of pellicles in extreme ultraviolet lithography”, *J.Kor.Phys.Soc.* 61, 1093 (2012).

[3] L. Scaccabarozzi *et al.,* “Investigation of EUV pellicle feasibility”, *Proc. SPIE,* Vol. 8679, 867904 (2013).

[4] F. Dhalluin *et al.* “Grid-supported EUV pellicles: A theoretical investigation for added value”, *Proc. SPIE*, Vol. 9658, 96580J (2015).

[5] I-S .Kim, M. Yeung, E. Barouch and H-K. Oh, “Impact of deformed extreme-ultraviolet pellicle in terms of CD uniformity”, *Proc. SPIE*, Vol. 9658, 96580K (2015).

[6] C. Zoldesi *et al.*, “Progress on EUV Pellicle development”, *Proc. SPIE,* Vol. 9048, 90481N (2014).

[7] E. Gallagher, J. Vanpaemel, I. Pollentier, H. Zahedmanesh, C. Adelmann, C. Huyghebaert, R. Jonckheere and J.U. Lee, “Properties and performance of EUVL pellicle membranes”, *Proc. SPIE*, Vol. 9635, 96350X (2015).

[8] S. Kwon, Y. Jung, H. Jeon, J. Kim, J. Choi, B-G. Kim and C.U. Jeon, “Thermal limitation of silicon EUV pellicle and possible improvements for mass production of EUV lithography”, International Symposium on Extreme Ultraviolet Lithography, 5-7 October 2015 (Maastricht, The Netherlands).

[9] D.L. Goldfarb, “Fabrication of a full-size EUV pellicle based on silicon nitride”, *Proc. SPIE*, Vol. 9635, 96350A (2015).

[10] V.A. Golyk, M. Krüger and M. Kardar, “Heat radiation from long cylindrical objects”, *Phys.Rev.E* 85, 046603 (2012).

[11] Y. Fan, S.B. Singer, R. Bergstrom and B.C. Regan, “Probing Planck’s Law with incandescent light emission from a single carbon nanotube”, *Phys.Rev.Lett.*102, 187402 (2009).

[12] S-G. Kim *et al.*, “Large-scale freestanding nanometer-thick graphite pellicles for mass production of nanodevices beyond 10 nm”, *Nanoscale (2015);* DOI:10.1039/C5NR03079J.

[13] C. Zoldesi *et al.*, “A pellicle solution for EUV”, International Symposium on Extreme Ultraviolet Lithography, 5-7 October 2015 (Maastricht, The Netherlands).

[14] C. Wuttke and A. Rauschenbeutel, “Thermalization via heat radiation of an individual object thinner than the thermal wavelength”, *Phys.Rev.Lett.* 111, 024301 (2013).

Downloaded From: http://proceedings.spiedigitallibrary.org/ on 03/24/2016 Terms of Use: http://spiedigitallibrary.org/ss/TermsOfUse.aspx

[15] D.L. Windt, “IMD - Software for modeling the optical properties of multilayer films”, *Comp. Phys.* 12, 360 (1998).
[16] Encyclopedia of Materials, Parts and Finishes (2nd Edition), edited by M.Schwartz, CRC Press (Boca Raton, FL 2005), p.708.
[17] N.M. Ravindra, S. Abedrabbo, W. Chen, F.M. Tong, A.K. Nanda and A.C. Speranza, “Temperature-dependent emissivity of silicon-related materials and structures”, *IEEE Trans. Semicond. Manufact*. 11, 30 (1998).
[18] T.J.R. Hughes, The Finite Element Method: Linear Static and Dynamic Finite Element Analysis, Dover Publication (Mineola, NY, 2000).
[19] A. Logg and G.N. Wells, “DOLFIN: Automated Finite Element Computing”, *ACM Transactions on Mathematical Software*, 37 (2010); doi:10.1145/1731022.1731030.
[20] A. Logg, K.-A. Mardal, G.N. Wells *et al*., *Automated Solution of Differential Equations by the Finite Element Method*, Springer (2012); doi:10.1007/978-3-642-23099-8.
[21] C.H. Mastrangelo, Y.-C. Tai, and R.S. Muller, “Thermophysical properties of low-residual stress, silicon-rich, LPCVD silicon nitride films”, *Sens. Actuators* A23, 856, (1990).
[22] A. Kaushik, H. Kahn and A.H. Heuer, “Wafer-level mechanical characterization of silicon nitride MEMS”, *J. Microelectromech.Syst.* 14, 359, (2005).
[23] M.T. Alam, M.P Manoharan, M.A. Haque, C. Muratore and A.Voevodin, “Influence of strain on thermal conductivity of silicon nitride thin films”, *J. Micromech.Microeng*. 22, 045001, (2012).
[24] A.I. Fedorchenko, A-B. Wang, V.I. Mashanov, W-P. Huan and H.H. Cheng, “Strain-induced wrinkling on SiGe free standing film”, *Appl. Phys. Let.* 89, 043119 (2006).
[25] N. Damil, M. Potier-Ferry and H. Hu, “Membrane wrinkling revisited from a multi-scale point of view”, *Advanced Modeling and Simulation in Engineering Sciences,* 1:6 (2014) ; doi:10.1186/2213-7467-1-6.

Downloaded From: http://proceedings.spiedigitallibrary.org/ on 03/24/2016 Terms of Use: http://spiedigitallibrary.org/ss/TermsOfUse.aspx